JOURNAL OF MATERIALS SCIENCE 23 (1988) 3129–3136

The elevated-temperature dependence of fracture energy mechanisms of hybrid carbon–glass fibre reinforced composites

M. MUNRO, C. P. Z. LAI*
Department of Mechanical Engineering, University of Ottawa, Ottawa, Canada

The fracture energy of a model hybrid carbon–glass–epoxy resin composite system has been evaluated at room temperature and three elevated temperatures. Values of the work of fracture increased with temperature and glass fibre content with an especially dramatic increase for the high temperature–high glass fibre content specimens. Evaluation of existing microstructural fracture energy mechanisms of fibre debonding, post-debond sliding and fibre pull-out were successful in quantitatively accounting for the work of fracture at room temperature. For the elevated-temperature tests of glass fibres in epoxy resin, it was shown that extensive frictional energy of the nature of the post-debond sliding mechanism is also dissipated after fibre failure.

1. Introduction

It is well known that the energy required to fracture a unidirectional fibre composite transversely to the fibre direction is not simply the sum of the weighted (according to volume fraction) fracture energies for the resin and fibre. Clearly, there are significant interactions between the fibre and the matrix at the interface. This fact has led to the development of a large number of additional fracture energy mechanisms [1]. It is generally agreed that the fibre pull-out mechanism [2, 3] accounts for the observed fracture energy of carbon fibre reinforced thermosetting resins [4–6]. The situation for glass fibre reinforced thermosetting resins is more disputed in that a single or multiple mechanisms have been proposed. These include fibre debonding [7], fibre pull-out [8], post-debond sliding [3, 9], and combinations of these three mechanisms [5, 6, 10, 11]. The above papers have covered a wide range of fibres, thermosetting resins and curing schedules which must result in different fibre–matrix interface conditions. This perhaps explains the disagreements over the relative importance of the individual failure mechanisms for glass fibre reinforced thermosetting resins.

This paper is an extension of two previous papers that studied parameters affecting the fracture energy mechanisms of hybrid carbon–glass fibre reinforced epoxy resin composites at room temperature; namely, the effects of carbon to glass fibre ratio [5] and testing rate (quasi-static or impact) [11]. In addition, analyses of the fracture mechanisms for two glass fibre composite systems (in which the glass fibre volume fraction was varied) were reported [10, 11]. Very similar conclusions regarding the relative importance of the fracture energy mechanisms were drawn in the studies: (i) the pull-out energy of carbon fibres in epoxy resins was linear with the amount of carbon fibre and fully accounted for the values obtained for the work of fracture; (ii) for glass fibres in epoxy resin, the fibre debonding and pull-out energies were similar in magnitude, while the post-debond friction energy was by far the dominant term and generally explained the non-linear behaviour exhibited by the work of fracture curve.

The consistent dominance of the post-debond friction energy term has resulted in additional investigations. The energy equation for this mechanism can be expressed as [5]

$$\gamma_{pdf} = \frac{V_f \sigma_f y^2 \Delta\varepsilon}{8\bar{l}} \quad (1)$$

It is of value to comment on each of these parameters. The volume fraction, V_f, and fibre failure strength, σ_f, are known values. The fibre debonded length, y, and the fibre pull-out length, $\bar{l}$, can be measured using the projection–reflection microscope technique [5]. Because of the potential significance of the squared dependence of the debond length, y, for the post-debond friction energy, an initial study was performed in which the debonded length was measured as a function of the mid-point deflection of a three-point bending beam specimen [10]. The results indicated a linear relationship between the debonded length and mid-point deflection, once a relatively small threshold mid-point deflection had been exceeded. Finally, the $\Delta\varepsilon$ term, which essentially represents the amount of relative sliding against an interfacial frictional shear stress between the fibre and matrix after debonding, has not been measured and has generally been assumed to be a constant value in all of the studies which evaluated post-debond friction energy. Kirk *et al.* [5] assumed a constant value of 0.01 for hybrid glass and carbon fibre epoxy resin composites. Beaumont and Anstice [6] assumed the same value for their studies on hybrid

* *Present address*: Dow Chemical (Hong Kong) Ltd, Tsing Yi Research and Development Laboratory, Hong Kong.

0022–2461/88 $03.00 + .12 © *1988 Chapman and Hall Ltd.*

glass and carbon polyester resin fibre composites. Wells and Beaumont [12] reported a similar approach in that $\Delta\varepsilon$ was estimated as the ratio of fibre strength to fibre modulus. In each of the above studies the estimate of $\Delta\varepsilon$ was empirical in nature and was assumed to be independent of the relative amount of carbon fibre and glass fibre in the hybrid composites. Thus, in order to understand the nature of and more accurately quantify the post-debond friction energy term, the nature of the $\Delta\varepsilon$ term was investigated.

The $\Delta\varepsilon$ term is generally assumed to be a measure of the amount of relative movement between the fibre and matrix after fibre debonding but prior to fibre fracture, i.e. the difference between fibre failure strain and matrix failure strain [3]. For typical elevated operating temperatures of fibre composites, the fibre failure strains would be similar to the room-temperature values. Since the failure strain of the matrix would change with elevated temperature, investigating the elevated-temperature behaviour of the hybrid composites would provide valuable insight into the $\Delta\varepsilon$ term. Besides providing details of the nature of the $\Delta\varepsilon$ term, the elevated-temperature dependence of the other fracture energy mechanisms of hybrid composite specimens would also be obtained. Thus, the experimental procedure selected was to fabricate and test hybrid carbon–glass fibre composites and neat resin specimens at elevated temperatures of 50, 65 and 80° C as well as at room temperature (23° C) [13, 14].

2. Experimental procedure

2.1. Materials and model specimen preparation

Unidirectional hybrid tapes containing various ratios of E-glass fibre strands and Grafil E/XA-S carbon fibre tows were obtained from Carr Reinforcements, Winsford, Cheshire, UK. The fibre properties are given in Table I. The glass fibre strands and carbon fibre tows from the tapes were used to fabricate model specimens with different ratios (by volume) of carbon to glass fibres. The arrangement of the fibre strands and tows for the six specimen groups is shown in Fig. 1. The matrix employed was Shell Epon 828 epoxy resin with a BF_3MEA complex hardener, Pacific Anchor Ancamine 1222 (12 phr) (Richmond, California). This particular hardener was selected as the resin and hardener mixture and had a six-month pot life at room temperature. Thus it was possible to prepare sufficient matrix for all the individual plates which were then cast at different times. This would eliminate any variation in results due to a variation in the ratio of resin to hardener.

The specimen fabrication procedure began with the casting of the individual specimen plates. Individual

TABLE I Fibre properties

Fibre type	Strand/tow tex	Tensile strength (GPa)	Tensile modulus (GPa)
E-glass	600	1.65*	70†
Graphil E/XA-S	600	3.15‡	246‡

*Determined by strand tensile tests.
†Manufacturer's data.
‡Determined by flat-bar tensile tests.

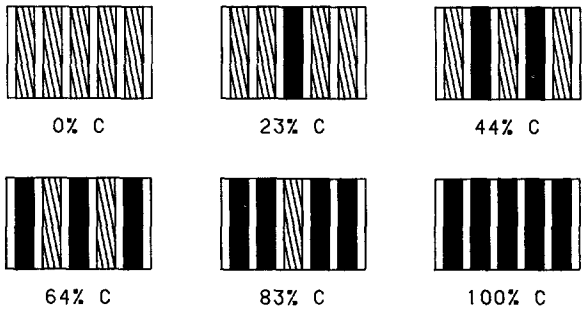

Figure 1 Arrangement of fibre bundles for model hybrid carbon–glass fibre specimens. Carbon tows are represented by dark bands.

strands and tows were placed in parallel machined grooves of a brass mould. Steel plates weighing 75 g were then attached to the end of each bundle. The machined grooves and constant tension helped to ensure constant spacing and alignment. Matrix preheated to 50° C was then poured into the preheated (50° C) brass mould. The filled mould was then subjected to vacuum (~ 25 torr) for 10 min to remove air bubbles and assist in fibre wetting. The assembly was then cured in normal atmosphere for a cure cycle of 2 h at 150° C followed by 2 h at 175° C.

Three-point bending beam specimens (Fig. 2) of dimensions 30.0 ± 0.5 mm long by 10.3 ± 0.1 mm wide by 3.0 ± 0.1 mm thick were machined from the cured plates. A slot (0.2 mm wide by 0.1 mm deep) was machined at the mid-point of the specimen at right-angles to the fibre direction in the subsequent tensile face of the specimen to aid in crack propagation. It should also be noted that the fibre bundles were placed as close to the tensile face of the specimen as possible to promote the tensile failure mode associated with the failure mechanisms. The specimens were then inspected and any that had splayed fibre bundles or had fibre bundles that deviated more than 3° from the longitudinal specimen axis were not tested. Prior to testing, the tensile faces of the specimens were polished with 0.3 μm alumina powder in order to be able to clearly measure the debonded zones. A razor blade was run along the bottom of the machined slot in order to create an initial sharp crack.

2.2 Model specimen testing

The model specimens were tested in three-point bending at a crosshead speed of 2.8 cm min^{-1} and at a span of 2.0 cm on an Instron testing machine (Model

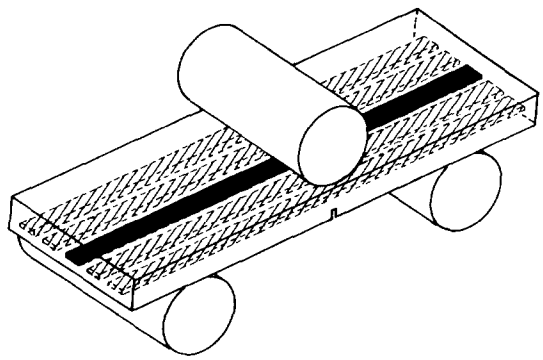

Figure 2 Three-point bending beam specimen [5].

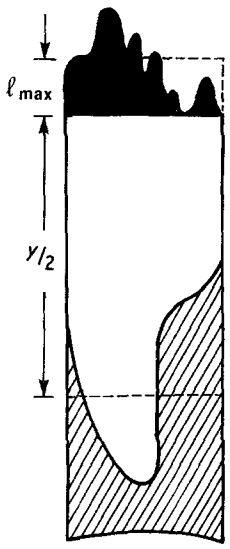

Figure 3 Pull-out and debonded lengths.

TTCM) equipped with a 5000 N load cell. The selected temperature environments of 23, 50, 65 and 80° C were provided by an Instron environmental chamber (Model 3111). A digital thermometer probe was placed at the mid-point of a reference specimen in a longitudinally bored hole to ensure that the specimens had reached the desired testing temperature. Seven to nine specimens were tested for each of the six hybrid groups at the four selected temperatures, resulting in a total of 187 specimens.

2.3. Measurement of debonded and pull-out lengths

The debonded lengths y and pullout lengths l_{max} of the fractured specimen (Fig. 3) were determined in the manner employed in the original study [5] using a projection microscope. When the specimen was viewed in the transmission mode, the protruding pulled-out fibres were clearly visible against a lighter background. A tracing was then made by following the dark outline of the fibre ends. A planimeter was used to determine the area of the tracing above the fracture plane, and the average fibre pull-out length for each tow end l_{max} was calculated by dividing this area by the width of the tow. When the microscope was used in the reflection mode, the debonded lengths of the fibres were clearly visible against a darker background and the average debonded length, y, was similarly obtained. A total of 2805 debonded and pull-out lengths were measured in this study. It was confirmed by viewing sectioned specimens that the glass fibres did undergo single-fibre debonding that was constant through the thickness, and not bundle debonding as investigated by Wells and Beaumont [15].

2.4 Tensile testing of neat resin specimens

The tensile failure strains and moduli required for subsequent calculations of the $\Delta\varepsilon$ term were determined for the neat resin at the selected test temperatures of 23, 50, 65 and 80° C. Neat resin plates sufficient for five tensile specimens were fabricated with the same resin and hardener and cure cycle as for the model specimen plates. Tensile specimens (ASTM Standard D638M-81) were then machined from these plates. The testing equipment was identical to that of the model specimens with the exception that an Instron extensometer was used to measure the tensile strain in the gauge length.

Since the bulk resin properties are sensitive to strain rate, particularly at elevated temperatures, an estimate of the model specimen longitudinal strain rate as a function of the testing machine crosshead rate used in the three-point bonding beam tests of the model specimens was made according to ASTM D790-81, using the equation

$$\dot{\varepsilon} = \frac{12c}{L^2}\dot{\delta} \tag{2}$$

where $\dot{\varepsilon}$ = tensile strain rate, c = estimate of the average distance from the neutral axis of the specimen to the centre of fibre bundles (0.06 cm), L = testing span of the model specimen (2.0 cm) and $\dot{\delta}$ = testing machine crosshead rate (2.8 cm min^{-1}). The tensile testing strain rate for the bulk specimens was thus selected at the nearest available value of approximately 0.65 min^{-1}.

3. Experimental results and discussion

3.1. Work of fracture

The energy required to completely fracture the specimen into two pieces, U, was equated to the area under the stress–strain curve (Fig. 4a). The drop in the stress–strain curve at Point A is associated with rapid crack propagation from the base of the machined slot to the fibre bundles which act as crack arrestors (Fig. 4d). Thus, the crack that passes though the fibre bundles is a propagated one rather than a machined crack.

The span of 2 cm was selected in the original study [5] to minimize stored elastic energy in the specimen and testing machine. In many cases the stored elastic energy was equal to the energy required to fracture the specimen into two pieces. For the specimens that did fly apart due to excess stored elastic energy, the kinetic energy calculated from the trajectory was insignificant; thus, within specimen groups the failure energies for both failure modes were very similar.

The experimental fracture energy (work of fracture), γ_f, was calculated using the equation

$$\gamma_f = \frac{U}{2A} \tag{3}$$

where A is the total cross-sectional area of the fibre bundles. The values of the work of fracture for the four selected temperatures and the six ratios of carbon fibre to glass fibre (expressed as volume percentage of carbon fibre in total fibre) are given in Fig. 5. The results indicate that the work of fracture increased as the temperature and the percentage of glass fibre increased. There was an especially dramatic increase in the work of fracture for the 100% glass fibre specimens tested at 80° C.

3.2. Evaluation of the theoretical fracture mechanism energies

The theoretical fracture energy mechanisms evaluated

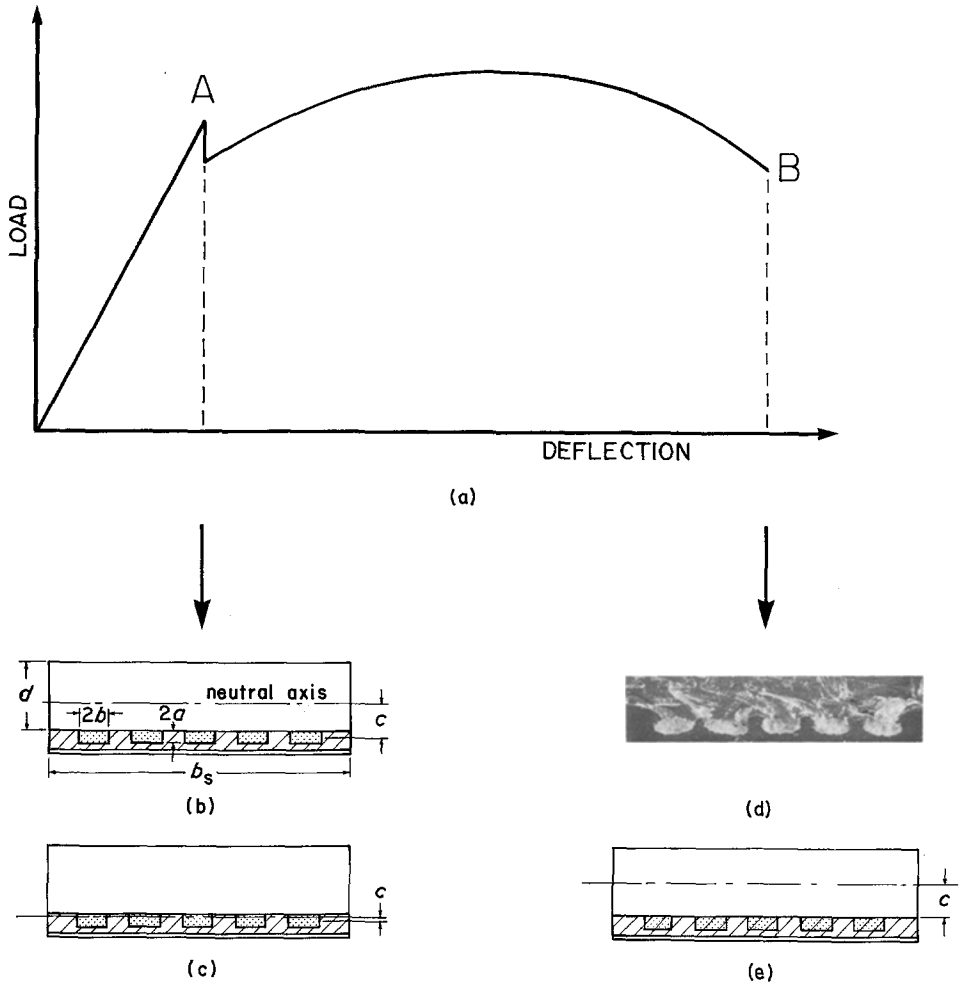

Figure 4 (a) Schematic load–deflection curve for the three-point bending beam test. (b) Idealized specimen cross-section for initial crack propagation (Point A) to the fibre bundles, where the neutral axis is located above the fibre bundles. (c) As in (b) except that the neutral axis passes through the fibre bundles. (d) Photograph of the cross-section of a 100% glass fibre composite model specimen, showing regions of initial rapid crack propagation (below fibre bundles) and the extent of crack blunting by the glass fibre bundles. (e) Idealized specimen cross-section after the crack has propagated past the fibre bundles (Point B).

in this paper (Table II) are the same as those of the previous four studies [5, 6, 10, 11]. The pull-out and debonded lengths were determined as described in Section 2.3 and together with other known properties (V_f, E_f, σ_f) were substituted into the equations of Table II.

The $\Delta\varepsilon$ term was the only parameter that remained to be evaluated. It was observed, as was mentioned earlier, that after initiation of the crack at Point A of Fig. 4a the propagating crack was arrested at the fibre bundles. It has been shown that essentially no debonding had occurred at this point [10, 14]. As the loading continued past this point, debonding of the fibre–matrix interface increased linearly with mid-point deflection of the specimen. At Point B the crack had completely propagated through the fibre bundles. At that point the stored elastic energy in the specimen and testing machine generally caused catastrophic

TABLE II Theoretical models of energy absorption fracture mechanisms

Model	Equation*	Ref.
Debonding energy	$\gamma_d = \frac{V_f \sigma_f y^2}{4E_f}$	[7]
Post-debond friction energy	$\gamma_{pdf} = \frac{V_f \sigma_f y^2 \Delta\varepsilon}{8\bar{l}}$	[5]
Pull-out energy	$\gamma_p = \frac{V_f \sigma_f \bar{l}}{6}$	[5]

* V_f = volume of fraction of carbon or glass fibres in total fibre, σ_f = ultimate strength of carbon or glass fibres, $\bar{l}$ = average pull-out length ($l_{max}/2$), E_f = Young's modulus of carbon or glass fibres, y = average debonded length, $\Delta\varepsilon$ = differential failure strain between fibre and matrix.

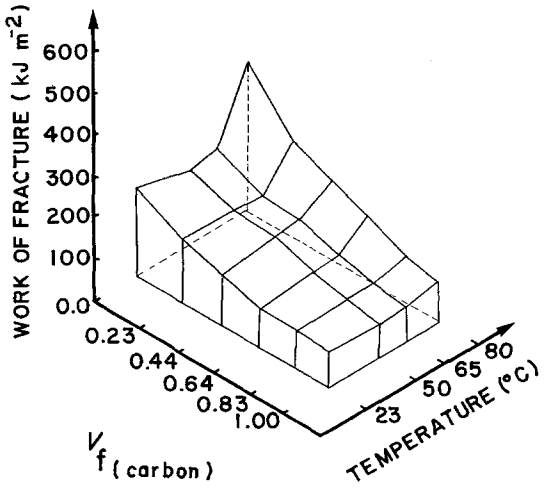

Figure 5 Work of fracture of model hybrid carbon–glass specimens as a function of carbon-fibre volume fraction and temperature.

TABLE III Variations of failure strain and modulus of near resin with temperature

Testing temperature (°C)	Failure strain (%)*	Young's modulus (GPa)*
25	0.045 ± 0.005	2.75 ± 0.29
50	0.048 ± 0.008	2.54 ± 0.28
65	0.064 ± 0.015	2.00 ± 0.22
80	0.188 ± 0.031	1.10 ± 0.16

*Mean ± standard deviation (five specimens).

failure of the remaining resin beam and thus complete specimen failure.

In order to obtain an experimentally determined estimate of the $\Delta\varepsilon$ term, the tensile strains in the glass fibre bundles at Points A and B were calculated using bending-beam theory.

The relationship between tensile strain in the fibres, ε, and crosshead displacement, δ, is given from ASTM D790-81 by the equation

$$\varepsilon = \frac{12c}{L^2}\delta \tag{4}$$

where c is the distance from the centre of the fibre bundles to the neutral axis (Figs 4b, c and e). The position of the neutral axis depends upon the elastic moduli of the resin and fibres and the relative amount of the fibre and unfractured resin. For the cases of the lower temperatures and high glass fibre content specimens, the neutral axis was above the fibre bundles (Fig. 4b). The location of the neutral axis at Point A was therefore determined by equating the products (above and below the neutral axis) of the axial stiffness (i.e. EA) of the fibres and/or resin times the distance from the neutral axis to the respective mid-points:

$$E_m(t)(d - c)b_s\left(\frac{d - c}{2}\right) = E_m(t)(c - a)b_s\left(\frac{c - a}{2}\right) + c\sum_{i=1}^{5} A_iE_i \tag{5}$$

where a = one-half the thickness of the fibre bundles (0.2×10^{-3} m), b = one-half the width of the fibre bundles (0.5×10^{-3} m), b_s = width of the model specimen (10.3×10^{-3} m), c = distance from mid-plane of fibre bundles to the neutral axis, $d = 2.4 \times 10^{-3}$ m, A_i = area of one fibre bundle ($4ab$) and $E_m(t)$ = elastic modulus of matrix at the selected temperature t and $E_i = E_fV_f + E_m(t)V_m$. The resulting value of c is

$$c = \frac{1}{2}\frac{bE_m(t)(d^2 - a^2)}{bE_m(t)(d - a) + \sum_{i=1}^{5} A_iE_i} \tag{6}$$

If the computed value of c was less than the distance a, then the neutral axis passed through the fibre bundles (Fig. 4c) and the value of c may be calculated from the equation

$$c = \frac{1}{2}\frac{E_m(t)(d - a)^2}{\sum_{i=1}^{5} A_iE_i} \tag{7}$$

As indicated in Figs 4b and c the shaded portions of the resin between the fibre bundles were not accounted for, as this resin had generally fractured when the crack was arrested at the fibre bundles (Fig. 4d). The stiffness of the resin included the variation of resin moduli with temperature (Table III) as determined by the elevated-temperature tensile testing of the neat resin specimens. The location of the neutral axis at Point B was in the middle of the unfractured resin as indicated in Fig. 4e. Since a unique load–deflection trace was produced for each specimen, the tensile strains (ε_A, ε_B) were determined for each of the 187 specimens.

The first estimate of $\Delta\varepsilon$, $\Delta\varepsilon_0$, was suggested by the original concept of the post-debond sliding mechanism which operated from the beginning of debonding to fibre fracture. Thus, the original $\Delta\varepsilon$ term was estimated as the average of the difference between the glass fibre failure strain (0.0236) and the tensile strain ε_A. For four of the eight specimens of the 100% glass fibre at 80° C group, the values of ε_A were greater than 0.0236 and thus resulted in negative $\Delta\varepsilon_0$ values. For these specimens the value of $\Delta\varepsilon_0$ was set to zero. The values of $\Delta\varepsilon_0$ are plotted as a function of composition and temperature in the lower portion of Fig. 6. The results indicate that the previously assumed value of $\Delta\varepsilon = 0.01$ for room-temperature testing of glass-fibre composites [5, 6, 10, 11] was indeed a reasonable value. For higher temperature tests of the predominantly glass-fibre composites, the value of $\Delta\varepsilon_0$ drops

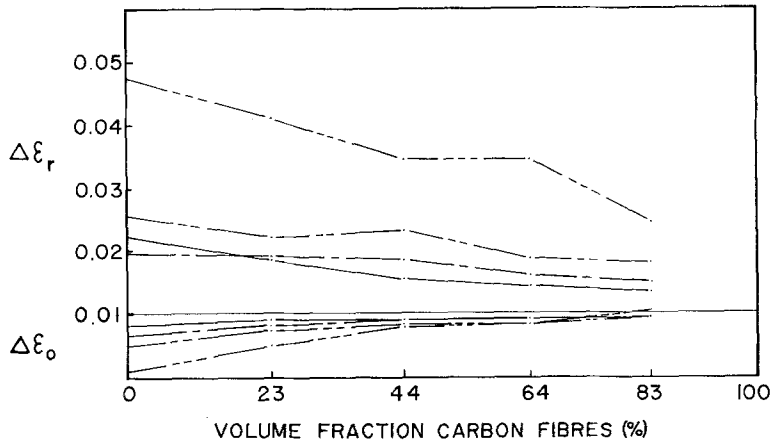

Figure 6 Measured differential strains of model hybrid carbon–glass fibre specimens as a function of carbon-fibre volume fraction and temperature; subscripts o and r represent original and revised concepts, respectively. (——) 23° C, (– – –) 50° C, (– – –) 65° C, (– – – –) 80° C.

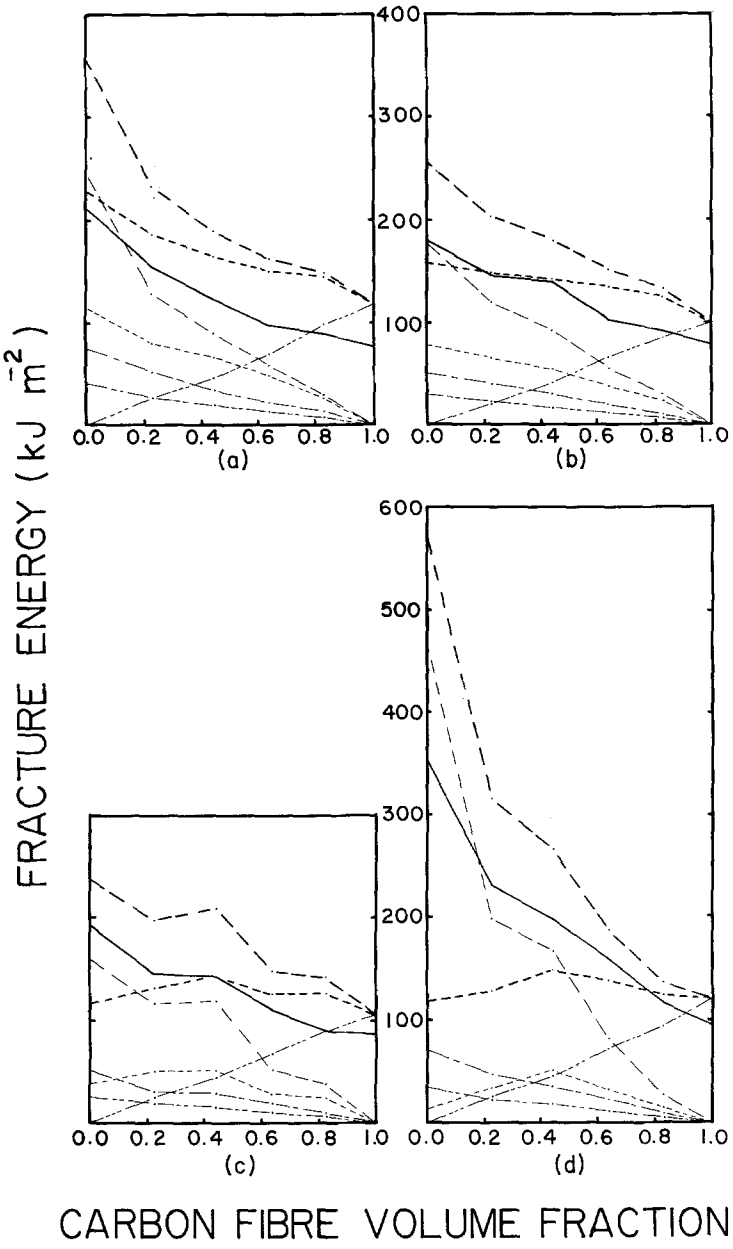

Figure 7 Fracture energy terms of model hybrid carbon–glass fibre specimens as functions of composition and testing temperatures of (a) 23° C, (b) 50° C, (c) 65° C and (d) 80° C. (——) Work of fracture, (– – –) total theoretical (original), (— — —) total theoretical (revised), (– – – –) glass post-debond friction (original), (– – –) glass post-debond (revised), (– – –) glass pull-out, (– – –) glass debond, (– – – –) carbon pull-out.

significantly due to the larger values of ε_A that were experimentally measured.

Assuming that the contributions to the fracture energy of the resin and fibres is negligible, the total theoretical fracture energy is [5, 11]

$$\gamma_T = (\gamma_p)^c + (\gamma_d)^g + (\gamma_{pdf})^g + (\gamma_p)^g \quad (8)$$

where the terms are as defined in Table II and the superscripts c, g refer to carbon and glass fibre, respectively. The computed individual and total theoretical fracture energies as functions of carbon fibre volume fraction and temperature are given in Fig. 7.

Some of the results for this study are, in general, similar to those of previous studies employing this approach. For all four testing temperatures, the glass fibre pull-out and debonding energies are linear with the volume fraction of glass fibres, with the pull-out energy consistently being greater than the debonding energy. In previous studies the glass fibre pull-out and debonding energies were similar in magnitude although, if there was a difference, the pull-out energy was the larger. The carbon fibre pull-out energy was again linear with carbon fibre volume fraction and accounted for the experimentally measured values of the work of fracture. In addition, it can be seen that the glass fibre debonding and pull-out results and the carbon fibre pull-out results are relatively independent of temperature. For the results of testing at 23° C, the glass fibre post-debond friction energy term based on $\Delta\varepsilon_0$ was the dominant term, and as before accounted for the variation in the total theoretical fracture energy curve. There was also good agreement between the total theoretical and experimental curves at 23° C. The agreement between these two curves decreased markedly as the testing temperature increased (Fig. 7) mainly due to the low values of $\Delta\varepsilon_0$. These low values indicated that there must be very little relative sliding between the glass fibres and the matrix. However, the specimens exhibited both significant values of the work of fracture and very high composite failure strains (up to ε_B values of 17% for 100% glass fibre composite specimens tested at 80° C). Thus, there must be extensive relative sliding between the glass fibres and the matrix at tensile strains above the assumed fibre failure strain of 0.0236 in order to account for the values of the work of fracture at elevated temperatures.

TABLE IV Work of fracture, fracture mechanisms and total theoretical fracture energies*

Testing temperature (°C)	Number of specimens	Carbon fibre volume fraction	Work of fracture ($kJ\,m^{-2}$)	Glass-fibre debond energy ($kJ\,m^{-2}$)	Revised glass-fibre post-debond friction energy ($kJ\,m^{-2}$)	Glass-fibre pull-out energy ($kJ\,m^{-2}$)	Carbon-fibre pull-out energy ($kJ\,m^{-2}$)	Revised total theoretical fracture energy ($kJ\,m^{-2}$)
23	8	0.00	231.7 ± 39.8	40.8 ± 5.8	245.3 ± 60.1	74.1 ± 16.5	0.0 ± 0.0	360.2 ± 68.1
	8	0.23	154.4 ± 29.4	27.0 ± 3.2	127.9 ± 43.1	52.8 ± 6.6	25.9 ± 3.3	233.5 ± 48.1
	7	0.44	123.5 ± 19.1	19.2 ± 3.0	89.4 ± 31.5	34.0 ± 5.5	45.5 ± 8.1	188.1 ± 38.1
	8	0.64	96.6 ± 11.7	13.2 ± 3.0	58.6 ± 22.8	21.9 ± 4.7	68.8 ± 8.7	162.5 ± 25.7
	7	0.83	89.5 ± 9.1	7.6 ± 1.0	28.6 ± 11.4	13.5 ± 3.3	98.1 ± 20.4	147.7 ± 24.3
	8	1.0	77.5 ± 9.5	0.0 ± 0.0	0.0 ± 0.0	0.0 ± 0.0	118.3 ± 19.6	118.3 ± 19.6
50	8	0.00	180.9 ± 27.6	29.8 ± 3.8	179.0 ± 52.7	49.7 ± 7.7	0.0 ± 0.0	258.5 ± 57.1
	8	0.23	145.0 ± 20.3	21.7 ± 4.1	118.4 ± 55.5	40.0 ± 4.4	21.0 ± 4.1	201.1 ± 60.7
	7	0.44	139.3 ± 23.1	16.5 ± 3.6	92.0 ± 50.2	29.3 ± 4.4	41.3 ± 5.0	179.1 ± 52.9
	8	0.64	102.8 ± 17.9	11.1 ± 2.4	54.6 ± 32.8	19.9 ± 4.2	65.6 ± 8.1	151.1 ± 39.8
	7	0.83	90.8 ± 9.9	6.2 ± 1.9	30.4 ± 21.1	10.3 ± 4.0	85.4 ± 33.6	132.4 ± 33.9
	9	1.00	76.8 ± 11.2	0.0 ± 0.0	0.0 ± 0.0	0.0 ± 0.0	99.2 ± 19.7	99.2 ± 19.7
65	8	0.00	193.0 ± 45.7	25.4 ± 5.4	161.1 ± 67.5	51.4 ± 7.6	0.0 ± 0.0	237.9 ± 79.7
	8	0.23	143.8 ± 21.7	19.6 ± 2.8	117.1 ± 35.5	35.0 ± 3.9	25.1 ± 6.2	196.0 ± 43.7
	7	0.44	141.8 ± 38.7	17.0 ± 6.1	118.9 ± 65.6	28.7 ± 8.8	45.2 ± 12.8	209.5 ± 84.1
	8	0.64	109.8 ± 19.3	10.1 ± 4.6	49.8 ± 35.9	19.5 ± 8.0	66.9 ± 13.3	146.3 ± 52.9
	9	0.83	89.2 ± 9.7	5.7 ± 1.5	37.7 ± 17.4	8.5 ± 2.8	88.5 ± 15.1	140.5 ± 29.6
	8	1.00	86.6 ± 10.3	0.0 ± 0.0	0.0 ± 0.0	0.0 ± 0.0	105.2 ± 20.0	105.2 ± 20.0
80	8	0.00	357.9 ± 85.9	35.0 ± 8.7	470.5 ± 270.7	71.0 ± 10.4	0.0 ± 0.0	576.4 ± 283.6
	8	0.23	234.3 ± 60.0	22.4 ± 4.9	219.4 ± 144.0	47.6 ± 8.8	25.8 ± 8.4	315.2 ± 158.1
	7	0.44	198.7 ± 44.0	18.3 ± 5.6	168.2 ± 95.3	34.7 ± 8.8	46.0 ± 10.1	267.2 ± 108.3
	8	0.64	160.3 ± 48.6	11.2 ± 3.9	81.8 ± 46.8	23.4 ± 6.4	72.6 ± 9.6	188.9 ± 57.0
	7	0.83	116.9 ± 20.8	4.9 ± 1.9	27.1 ± 17.7	10.4 ± 3.8	94.4 ± 6.2	136.8 ± 26.2
	8	1.00	96.4 ± 28.9	0.0 ± 0.0	0.0 ± 0.0	0.0 ± 0.0	122.2 ± 21.3	122.2 ± 21.3

*Mean ± standard deviation.

Considering the general concept that the $\Delta\varepsilon$ term represents the relative sliding between fibre and matrix after debonding, a second estimate of the relative sliding was therefore evaluated as

$$\Delta\varepsilon_r = \frac{\varepsilon_B - \varepsilon_A}{2} \quad (9)$$

The values of the revised $\Delta\varepsilon$ term, $\Delta\varepsilon_r$, as a function of composition and temperature are given in the upper portion of Fig. 6. The values are significantly larger than those for $\Delta\varepsilon_0$ and in general increase with increasing temperature. The revised post-debond friction energy was then calculated; however, the debonded length, y, of the post-debond friction energy equation was modified as in Equation 10 below in order that the frictional work associated with the pull-out length was not also counted in the revised post-debond friction energy term:

$$\gamma_{pdf_r} = \frac{V_f\sigma_f(y - \bar{l})^2\Delta\varepsilon_r}{8\bar{l}} \quad (10)$$

The values for the revised post-debond friction energy calculated using Equation 10 and the revised total theoretical energy curves are also shown in Fig. 7. In order to simplify the diagrams the standard deviations are listed in Table IV. For the elevated temperatures there was much better agreement in the magnitudes and trends exhibited by the work of fracture and the revised total theoretical fracture energy curves. Thus, at elevated temperatures, there must be extensive frictional work done of the nature assumed in the post-debond sliding mechanism at the interface after glass-fibre failure, in addition to that from the glass-fibre pull-out mechanism. Finally, the $\Delta\varepsilon$ term for the post-debond friction energy can be best estimated as the average of the specimen failure strain less the strain at the onset of debonding.

4. Conclusions

There are several conclusions that can be made concerning the results obtained from this study. Firstly, the temperature dependence of the energies associated with the failure mechanisms of hybrid carbon and glass fibre composites has been determined. As in several past studies, the post-debond friction energy term has been shown to be dominant. The second conclusion is directly related to the first in that the only previously unknown variable in the post-debond friction energy equation, $\Delta\varepsilon$, has been quantified. It has been shown that for elevated temperatures the $\Delta\varepsilon$ term is not constant as assumed in previous studies but is a function of the temperature, the relative amount of glass and carbon fibre in the hybrid composites, and the amount of relative sliding between glass fibres and matrix beginning at the onset of fibre debonding and lasting until complete failure. More importantly there must be extensive frictional work of the nature of the post-debond sliding type after glass-fibre failure, in addition to that from the glass-fibre pull-out mechanism.

Acknowledgement

The authors wish to thank the Natural Sciences and Engineering Research Council of Canada for their support of this work.

References

1. J. K. WELLS and P. W. R. BEAUMONT, *J. Mater. Sci.* **20** (1985) 2735.
2. A. H. COTTRELL, *Proc. R. Soc.* **A282** (1964) 2.
3. A. KELLY, *ibid.* **A282** (1964) 63.
4. P. W. R. BEAUMONT and B. HARRIS, *J. Mater. Sci.* **7** (1972) 1265.
5. J. N. KIRK, M. MUNRO and P. W. R. BEAUMONT, *ibid.* **13** (1978) 2197.
6. P. W. R. BEAUMONT and P. D. ANSTICE, *ibid.* **15** (1980) 2619.
7. J. O. OUTWATER and M. C. MURPHY, in Proceedings of 24th Annual Technical Conference, Composites Division, Society of Plastics Industry, New York (1969) Paper IIc.
8. B. GERSHOM and G. MAROM, *J. Mater. Sci.* **10** (1975) 1549.
9. M. R. PIGGOTT, *ibid.* **5** (1970) 669.
10. M. MUNRO and P. W. R. BEAUMONT, in Proceedings of 3rd International Conference on Mechanical Behaviour of Materials (1979) p. 253.
11. M. MUNRO, in Proceedings of the Strength and Fracture of Composites – Canadian Fracture Conference 4, Alton, Ontario, Canada, October (1980) p. 94.
12. J. K. WELLS and P. W. R. BEAUMONT, *J. Mater. Sci.* **17** (1982) 397.
13. C. P. Z. LAI, MASc thesis, University of Ottawa (1983).
14. M. MUNRO, unpublished results (1986).
15. J. K. WELLS and P. W. R. BEAUMONT, *J. Mater. Sci.* **20** (1985) 1275.

Received 3 July 1987
and accepted 27 January 1988